



# Geological factors and fracture distribution in deep and ultra-deep sandstones in Kuqa Depression, Tarim Basin, China

Yang Su<sup>1,2</sup>, Jin Lai<sup>1,2</sup>, Wenle Dang<sup>2</sup>, Xinjian Zhao<sup>3</sup>, Chuang Han<sup>3</sup>, Yongjia Zhang<sup>2</sup>, Zhongrui Wang<sup>2</sup>, Lei Wang<sup>2</sup>, Guiwen Wang<sup>1,2</sup>

<sup>1</sup>National Key Laboratory of Petroleum Resources and Engineering, China University of Petroleum (Beijing), Beijing, 102249, China

<sup>2</sup>College of Geosciences, China University of Petroleum (Beijing), Beijing, 102249, China

<sup>3</sup>Research Institute of Petroleum Exploration and Development, Tarim Oilfield Company, CNPC, Korla, 841000, Xinjiang, China

Correspondence to: Yang Su (suyangcupb@163.com)

**Abstract.** Deep and ultra-deep sandstone reservoirs hold great potential for hydrocarbon resources, yet complex geological challenges hinder the successful exploitation of oil and gas. Fractures in deep and ultra-deep sandstones are prevalent and significantly enhance rock permeability, and critically impact fluid flow and hydrocarbon productivity. Relationships between geological factors and fracture distribution in deep sandstone reservoirs, despite its significance, have remained poorly understood. This study utilizes core, thin section, acoustic emission tests and geophysical well logs to elucidate the interplay between geological elements and fracture occurrences in tight sandstones of the Kuqa Depression, which is a tectonically active foreland basin. The controls of sedimentation, sandbody distribution and earth stress on fracture distribution are analyzed. The research then unravels the effects of lithology units, earth stress fields, and broader tectonic context on fracture distribution patterns. Geological factors, including sedimentary factors (lithology, sandbody thickness and sandbody distribution), earth stress, and tectonic structure are integrated to comprehensively evaluate the fracture distributions in Kuqa Depression. The different lithologies are identified, and fractures in different lithologies are characterized. High-angle fractures and vertical fractures are mainly fracture types in Bozi-Dabei area. The fracture density increases as the sandbody thickness increases. The presence of thinner sandstones in conjunction with thin mud layers facilitates the formation of fractures. Paleostress affects the generation of natural fractures, and high fracture density is associated with high paleostress magnitudes. In situ stress affects the subsequent modification of natural fractures, and high in situ stress results in low fracture aperture. Structure factors including the position at folds and the proximity to faults are crucial for the fracture distribution. Fractures are more abundant in the hinge areas of anticlines compared to the limb areas, and fracture density above the neutral planes is notably higher. In addition, fracture density is higher in the formation adjacent to the fault due to the effect of the regional stress field. This study helps unravel the geological controlling factors and distribution of fractures by integrating geological and geophysical data, and has implications for hydrocarbon resource exploration in deep and ultra-deep sandstones.



## 1 Introduction

Fractures are prevalent in deep and ultra-deep reservoirs and fracture-induced heterogeneities can significantly increase permeability and productivity in rocks (Laubach, 2003; Ghosh and Mitra, 2009; Olson et al., 2009; Laubach et al., 2019; Chen et al., 2021; Cawood et al., 2023). Fractures in deep and ultra-deep tight sandstones have a major impact on fluid flow, controlling reservoir connectivity, and determining reservoir properties (Laubach, 2003; Zeng et al., 2013; Laubach et al., 2019; Zeng et al., 2023). Fractures play a crucial role in environmental and energy resource issues (Nelson et al., 1985; Gale et al., 2014; Ogata et al., 2017; Zhao et al., 2021; Zeng et al., 2023). Understanding the complex geological factors affecting fracture distribution in deep and ultra-deep sandstone reservoirs is essential for optimizing hydrocarbon recovery, improving reservoir delineation, and assessing risks effectively (Hank et al., 1997; Zeng, 2010; Launch et al., 2019; Feng et al., 2023; Zeng et al., 2023). Geophysical well logs including conventional well logs, image logs, and array acoustic logs provide crucial insights into the rock's physical properties, compositional variations, and structural discontinuities (Lyu et al., 2016; Pang et al., 2023; Lai et al., 2023; Lai et al., 2024; Zhang et al., 2024). A comprehensive approach integrating geological data and geophysical well logs can reveal relationships between geological factors and fracture distribution.

A growing body of research indicates that natural fractures are controlled by many factors including structural factors and sedimentary factors (Bogdonov, 1947; Nelson, 1985; Jamison, 1997; Feng et al., 2019; Douma et al., 2019; Sun et al., 2021; Zeng et al., 2023; Cawood et al., 2023). Due to complex interplay between structure (structural positions, fault, earth stress) and sedimentation (lithology, sandbody distribution), it makes it difficult to predict fracture occurrence and distribution (Friedman, 1969; Ghosh and Mitra, 2009; Frehner, 2011; Douma et al., 2019; Feng et al., 2019; Ogata et al., 2019; Zhao et al., 2021; Yang et al., 2021). There are multiple factors influence distribution of fractures in sandstones, and they include the inherent mechanical characteristics of lithological units, regional stress fields, and structure (Hank et al., 1997; Ghosh and Mitra, 2009; Frehner, 2011; Feng et al., 2019; Lai et al., 2019; Cawood et al., 2023). Earth stress regime is a pivotal determinant of fracture mechanics within tight sandstone reservoirs (Zeng et al., 2009; Lai et al., 2019; Guo et al., 2019; Zeng et al., 2023). The earth stress significantly dictates the initiation and progression of fractures in augmenting permeability and productivity of reservoirs (Lai et al., 2019; Guo et al., 2019; Zeng et al., 2023). Structure is the crucial factor controlling the fracture distribution (Friedman, 1969; Hanks et al., 1997; Jamison, 1997; Ghosh and Mitra, 2009; Cawood et al., 2023; Zeng et al., 2023). Apart from the thickness of sandstones and the lithology of the rocks, fracture density is also influenced by structural location, such as the proximity to fault, and is related to its location within the folds (Friedman et al., 1969; Jamison et al., 1997; Ghosh and Mitra, 2009; Ju et al., 2014; Sun et al., 2021; Cawood et al., 2023).

The Kuqa Depression is a foreland basin between the Tianshan Orogenic Belt and the Northern Tarim Uplift to the south in the Tarim Basin. Fractures are abundant in the deep and ultra-deep Cretaceous Bashijiqike Formation in Kuqa Depression due to the multiple stages of tectonic evolution. However, few studies are performed on clarifying geological factors and fracture distribution in Kuqa Depression using geological and geophysical well logs (Chen et al., 2021; Li et al., 2024). The study is designed to unravel the relationships between structure, lithological properties and fracture distribution in deep and ultra-deep



reservoirs in Kuqa Depression. The interplay between sandbodies and formation of fracture networks is analyzed, and this study elucidates the variability in fracture patterns. The well responses of different types of fractures are analyzed, and image logs are used to establish a set of criteria for fracture interpretation in different lithologies. This study then investigates the relationship among geological factors including lithology, sandbodies thickness, sandbodies distribution, earth stress, fault and tectonic positions. The methodologies for interpreting geophysical well log data are established to ascertain distribution of fractures within diverse structural settings and lithological units. The results will provide new insights into geological controlling factors of fractures and fracture distribution in deep and ultra-deep sandstone reservoirs using geological data and geophysical well logs.

## 2 Geological Settings

The Kuqa Depression is a segment of foreland basin that has undergone an intricate evolutionary history spanning Mesozoic and Cenozoic eras (Qiu et al., 2012; Yang et al., 2023). The structural configuration of Kuqa Depression is a testament to the dynamic interplay between northward drift of Indian subcontinent and southward compressive forces exerted by South Tianshan orogenic belt (Lu et al., 1994; Ju et al., 2014; Li et al., 2016; Nian et al., 2017) (Fig. 1). The Kuqa Depression contains three sags and four structural belts, including Baicheng, Wushi and Yangxia Sag, Northern monoclines, Kelasu, Qiulitage and Southern Gentle Monoclinical structural belts (Fig. 1) (Zeng, 2010; Qiu et al., 2012). The Kelasu belt is partitioned into five blocks including Awat block, Bozi block, Dabei block, Keshen block, and Kela block (Fig. 1). The structural trace of Bozi-Dabei block is an “S” shape (Fig. 1) (Guo et al., 2016; Yang et al., 2023).

Kuqa Depression has experienced three major stages, including a paleo-foreland stage, an extensional stage and a rejuvenated foreland stage (Zeng, 2010; Wu et al., 2019). The compressive tectonic movement within Bozi-Dabei zone began in Late Yanshan epoch and reached its peak intensity in Late Himalayan epoch (Li et al., 2016; Guo et al., 2016; Yang et al., 2023). The most intense tectonic movement occurred during the middle to late depositional phases of Kuqa Depression, significantly contributing to the formation of current structural configuration observed in Bozi-Dabei areas (Fig. 1) (Yu et al., 2014; Yang et al., 2023).

Triassic lacustrine mudstones and Jurassic coal-bearing strata as source rocks provide a bountiful hydrocarbon endowment. Paleogene Kmugeliemu and Neogene Jidike Formations as cap rocks help preserve oil and gas (Li et al., 2012; Zhao et al., 2022). The inception of regional uplift and erosion during Late Cretaceous has led to the stratigraphic absence of Upper Cretaceous deposits (Zhao et al., 2005; Jin et al., 2008). Lower Cretaceous strata of the region are characterized by Kapushaliang Group and Bashijiqike Formation, denoted as  $K_1bs$ . Kapushaliang Group includes Yageliemu Formation ( $K_{1y}$ ), Shushanhe Formation ( $K_{1s}$ ), and Baxigai Formation ( $K_{1b}$ ). Notably, Bashijiqike Formation, which serves as the principal hydrocarbon-bearing stratum, exhibits a conformable contact with subjacent Baxigai Formation. There is unconformable contact between Paleocene-Eocene Kumugeliemu Formation and underlying Cretaceous strata, indicating a significant absence in sedimentation (Zeng, 2010; Yu et al., 2016).



Due to the erosion of southern Tianshan Mountain, terrigenous clast was provided for Cretaceous reservoir deposition. The depositional environment of Bashijiqike Formation transitions from south to north and changes from a fan delta to a braided river delta (Nian et al., 2018; Zhang et al., 2021; Li et al., 2024). The lithologies of Bashijiqike Formation are mainly medium-grained sandstones, fine-grained sandstones, mudstones and in some cases conglomerates (Jia and Li, 2008; Lai et al., 2018).

100 Cretaceous Bashijiqike reservoir, which is buried in deep (>4500 m) and ultra-deep (>6000 m) depths, exhibits a low porosity and permeability. Owing to high overburden stress and intricate interplay of diagenetic processes, the sandstones are heavily fractured. The fractures provide hydrocarbon storage spaces and substantial enhancement of reservoir permeability (Nian et al., 2017; Sun et al., 2017; Zeng et al., 2023).



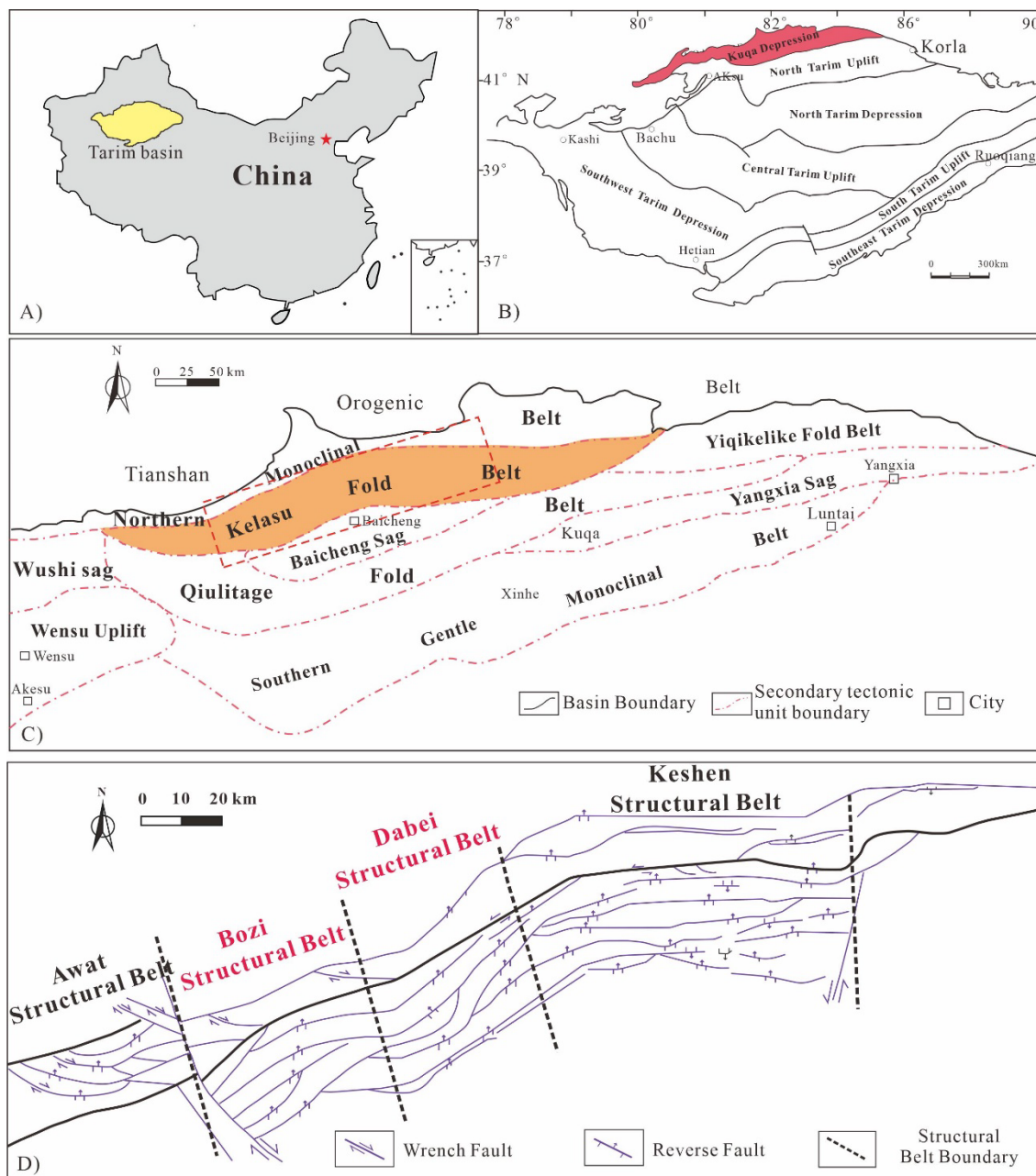


**Figure 1: (A) Geographic location of Tarim basin in China; (B) Geographic location of the Keshen Thrust Belt in Tarim basin; (C) the structural subdivision map of Kuqa Depression; (D) mapping locations of four zones in the Keshen Thrust Belt (Lai et al., 2021; Song et al., 2024)**



### 110 3 Materials and methods

Core samples, which are directly used to observe fracture occurrence and fracture distribution, are collected from 29 wells. The total length of cores can reach up to 284 meters.

Thin sections (30  $\mu\text{m}$  thick) were infused with blue-fluorescent epoxy resin to enhance the visibility of pores and microfractures. Additionally, thin sections were treated with a staining solution including Alizarin Red and potassium ferricyanide to identify different minerals. The distribution, orientation, and filling materials of microfractures can be analyzed by thin sections.

Acoustic emission Test (AE) at Sichuan University quantifies rock stress and infers historical stress conditions. This phenomenon is characterized by a significant increase in AE activity upon surpassing the stress threshold that induced irreversible deformation, such as the propagation of microfracture (Kaiser, 1953; Lavrov, 2003; Guo et al., 2019; Lai et al., 2019). The magnitude of paleostress can be obtained through AE tests.

Image logs provide high-resolution images of the borehole wall, which are essential for detailed geological analysis. A high-definition image log is utilized to capture images of the formation. The fracture characteristics can be observed and fracture parameters can be calculated by image logs. Formation MicroScanner Image (FMI) was run in most of the wells drilled in water-based muds. The workflow for processing FMI data includes Quality Control (QC), Speed Correction, Pad image creation-Button harmonization, Pad concatenation and orientation (creating a static image) and Histogram equalization-Pad concatenation and orientation (creating a dynamic image). Earth Imaging (EI) and QuantaGeo were run in the oil-based muds (Lai et al., 2024).

Array acoustic logs are a type of acoustic well logging that uses an array of transducers to measure the formation's acoustic properties. P-wave time difference, S-wave time difference, and Stoneley wave time difference can be obtained through array acoustic logs, including Dipole Shear Sonic Imager (DSI) and Cross-Multipole Array Acoustic Log (XMAC). The DSI tool (from Schlumberger) uses a combination of monopole and dipole transmitters along with an array of hydrophones to measure these wave velocities (Zahmatkesh et al., 2017). XMAC (from Baker Atlas) operates by combining a monopole array with a dipole array to capture detailed information on the formation's acoustic properties including compressional, shear, and Stoneley wave velocities, as well as amplitude attenuation.

The ECLIPS-5700 Series tools operate on a variety of measurement principles, including but not limited to natural gamma ray (GR), photoelectric (Pe) log, caliper (CAL), neutron porosity (CNC), bulk density (DEN), sonic interval transit time (DT), and High Definition Induction Resistivity logs (HDIL) (M2Rx, M2R9, M2R6, M2R3, M2R2, M2R1).

Ultrasonic imaging logging (UXPL) also is run in some wells drilled with oil-based muds. UXPL tool provides a high-resolution, 360° view of the borehole wall (Li et al., 2019). Fractures and borehole breakouts over the full circumference of the borehole can be identified by UXPL tool (Lai et al., 2018).



## 4 Results

### 4.1 Core-scale fractures

The types of fractures that can be observed on cores include low-angle fractures (Fig. 2A), horizontal fractures (Fig. 2B), vertical fractures (Fig. 2C), high-angle fractures (Fig. 2D, 2F, 2H) and network fractures (Fig. 2G). According to different filling cements, natural fractures can be divided into open fractures (Fig. 2B, 2D), semi-filled fractures (Fig. 2C, 2E, 2H) and filled fractures (Fig. 2A, 2F). Fracture observations from cores confirm that high-angle fractures and vertical fractures are the main fracture types in Bozi-Dabei area of Kuqa Depression. Most fractures have straight and smooth surfaces (Fig. 2). As a result of the intricate interplay of multi-phase tectonic processes, fractures intersect at varying angles, establishing fracture network (Fig. 2G). Occasionally fractures are visible cutting through the gravel (Fig. 2B). Open fractures can also be detected, and in some cases are filled with calcite (Fig. 2H, 2I).

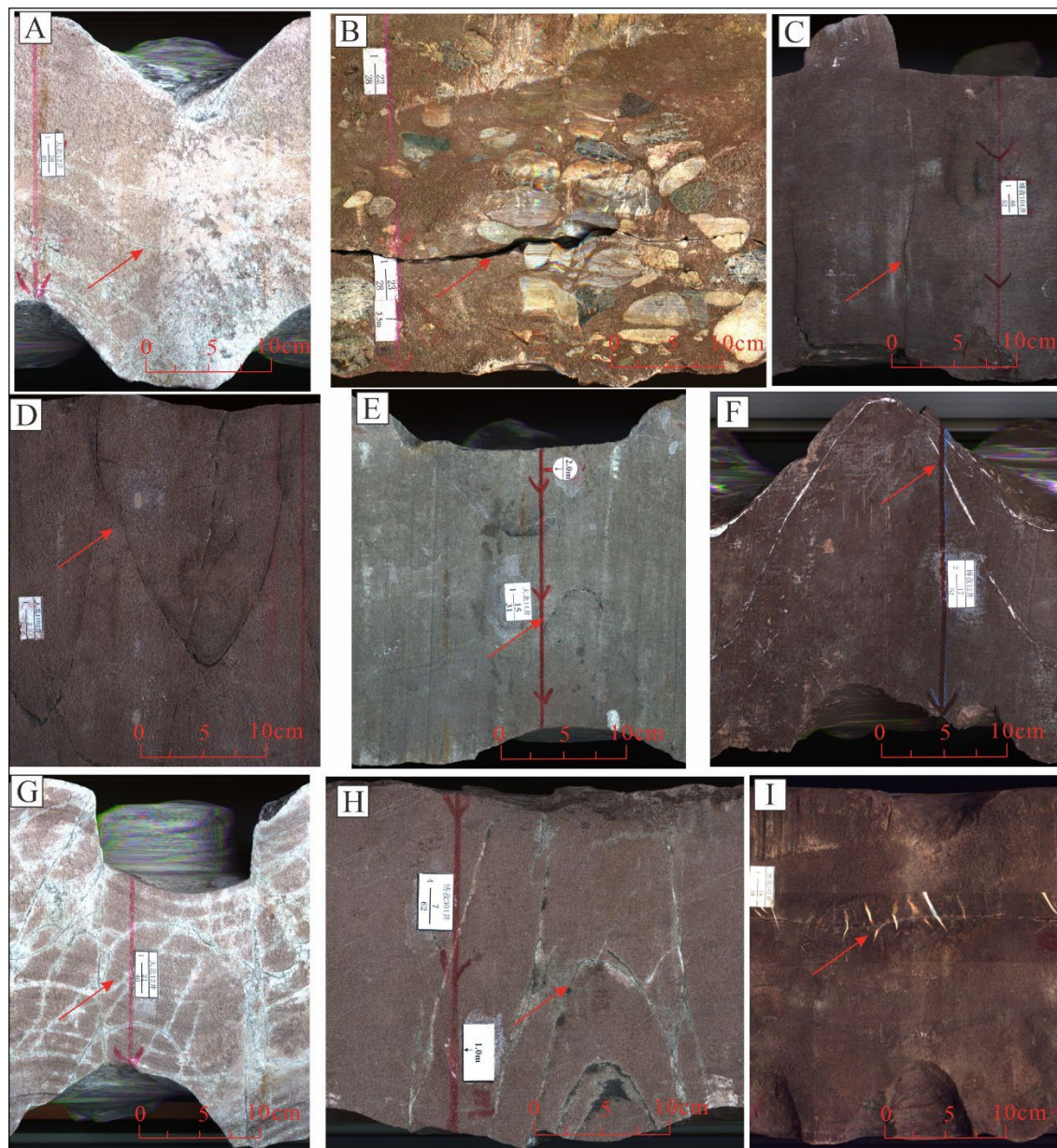


**Figure 2: The core photos of various types of core-scale fractures in Bashijiqike formation in Bozi-Dabei Blocks of Kuqa Depression**

- A. Closed (calcite filled) low-angle fracture, Well BZ 12
- B. Open horizontal fracture, Well BZ 1
- C. Vertical fracture, Well BZ 104
- D. High-angle fracture, Well DB 1102
- E. Filled fracture (undergo dissolution), Well DB 14





**F. Closed (calcite filled) fracture, Well BZ 12**

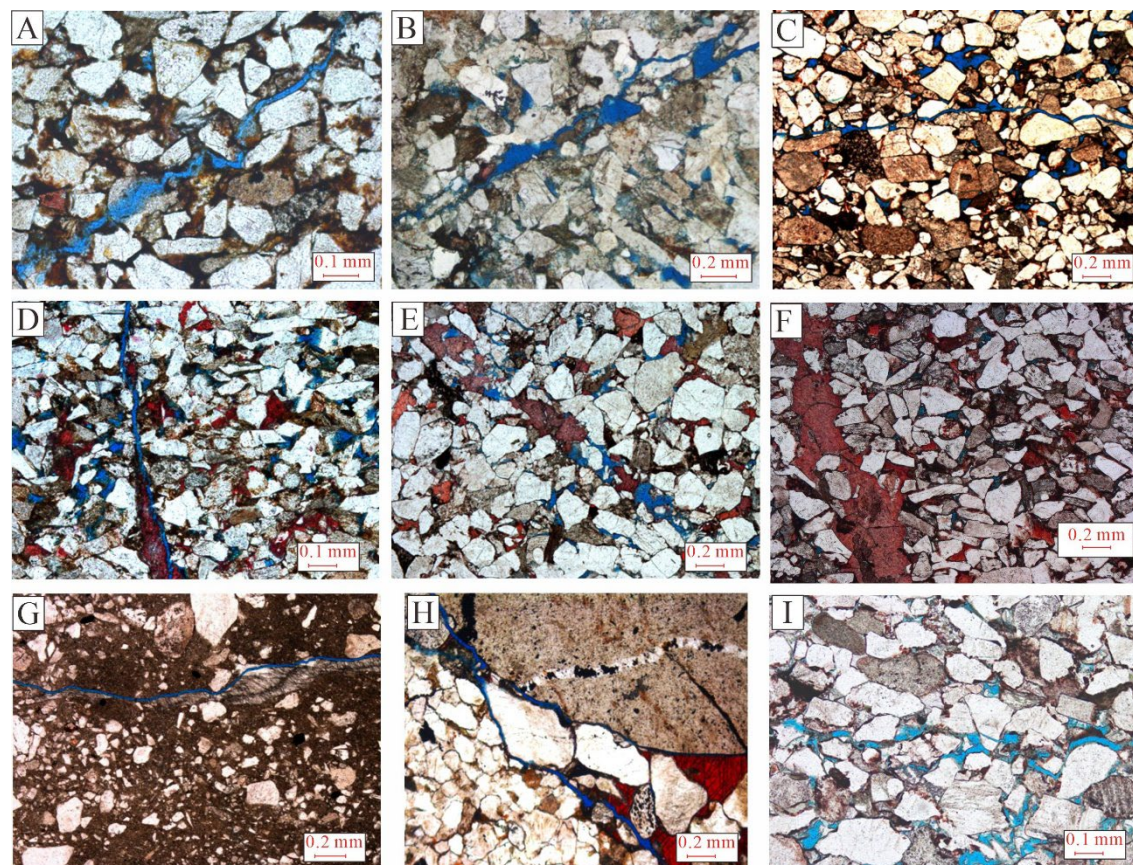
**G. Fracture network, Well DB 12**

160 **H. Combination of high-angle fracture with different angles, Well BZ 301**

**I. Open fracture, Well BZ 101**

#### **4.2 Thin section-scale micro-fractures**

Thin section images can reveal the characteristics of fractures in the micrometer scales. The aperture of micro-fractures varies from 0.01 to 0.04 mm. The aperture of small-scale fractures varies from 0.05 to 0.1 mm. Owing to  
165 the resolution limit of well logs, microfractures ( $< 0.1$  mm) can not be observed by well log data. The fractures that were detected in thin sections include micro-fractures and small-scale fractures (Fig. 3). The microfractures can be detected in the fine-medium grained sandstones (Fig. 3A-3C, 3E, 3F), siltstones (Fig. 3D) and in some cases conglomerates (Fig. 3H). Some intragranular microfractures are also related to tectonic compression (Fig. 3A, 3C, 3I). The fractures are partly to fully filled by calcite cements or dolomite cements (Fig. 3E-3G). The aperture of  
170 fractures with dissolution can get to 0.3 mm and be larger than the grain size of the rocks studied. However, the fractures with large apertures are mainly filled with calcite cements (Fig. 3F). The microfractures located at the grain boundary have the characteristics of narrow width (Fig. 3H). The fractures formed by dissolution can connect the intergranular and intragranular dissolution pores to form microfracture network (Fig. 3I).



175 **Figure 3: The thin section images of various types of thin section-scale fractures in Bashijiqike formation in Bozi-Dabei Block of Kuqa Depression**

- A. Microfracture which is formed by tectonism and dissolution, DB 903, 5178.7 m
- B. Microfracture and enlargement by dissolution, DB 902, 5099.19 m
- C. Microfracture crosscutting the framework grains, BZ 9, 7675.95 m
- 180 D. Microfracture fully cemented by calcite cements coexisting unfilled microfracture, DB 14, 6349.34 m
- E. Fracture partly cemented by calcite cements, DB 9, 4846.03 m
- F. Fracture fully filled by calcite cements, BZ 22, 6328.92 m
- G. Fracture fully filled by dolomite cements, BZ 12, 7001.9 m
- H. Grain boundary microfracture, BZ 302, 6186.85 m
- 185 I. Microfracture network which are formed by dissolution, BZ 104, 6802.14 m



### 4.3 Log responses of fractures

The presence of fractures in formations drilled with water-based muds is often indicated by a reduction of density logs. This reduction is particularly evident when fractures are filled with low-density materials such as drilling muds (Fig.4). Given that the velocity of acoustic waves is slower in liquids compared to solids, the identification of fractures through well logs is accompanied by an increasing interval transit time (AC readings) (Lyu et al., 2017; He et al., 2023) (Fig.4). For dual laterolog resistivity logging, the presence of fractures leads to a significant decrease in deep and shallow lateral resistivity values when fracture dip angle is small. The value of resistivity around borehole wall can be obtained by image logs. Natural fractures appear as sinusoidal wave appearance in image logs (Fig.4). If fractures are filled with low resistivity materials like water-based muds, fractures represent a dark sinusoidal wave appearance (Khair et al., 2015). If fractures are filled with high resistivity materials including oil-based muds, gypsum and carbonate cements, the fractures represent bright sinusoidal wave appearances. Meanwhile, the infiltration of muds into fractures leads to an increase in hydrogen content, which in turn, results in an increase in CNL log value (Lai et al., 2017).

The presence of conductive fractures in a formation significantly improves its permeability by providing pathways for fluid flow (Lai et al., 2017; Zeng et al., 2023). The fractures have an absorption and attenuation effect on acoustic waves, which leads to the attenuation of acoustic signals in dipole array sonic logs. The images of full waveforms were provided by array acoustic logging tools. The full waveforms exhibit “V” shape interferometric fringes and the amplitude as well as energy of full-wave waveform show significant attenuation with the presence of conductive fractures (Koerperich et al., 1978) (Fig. 4).



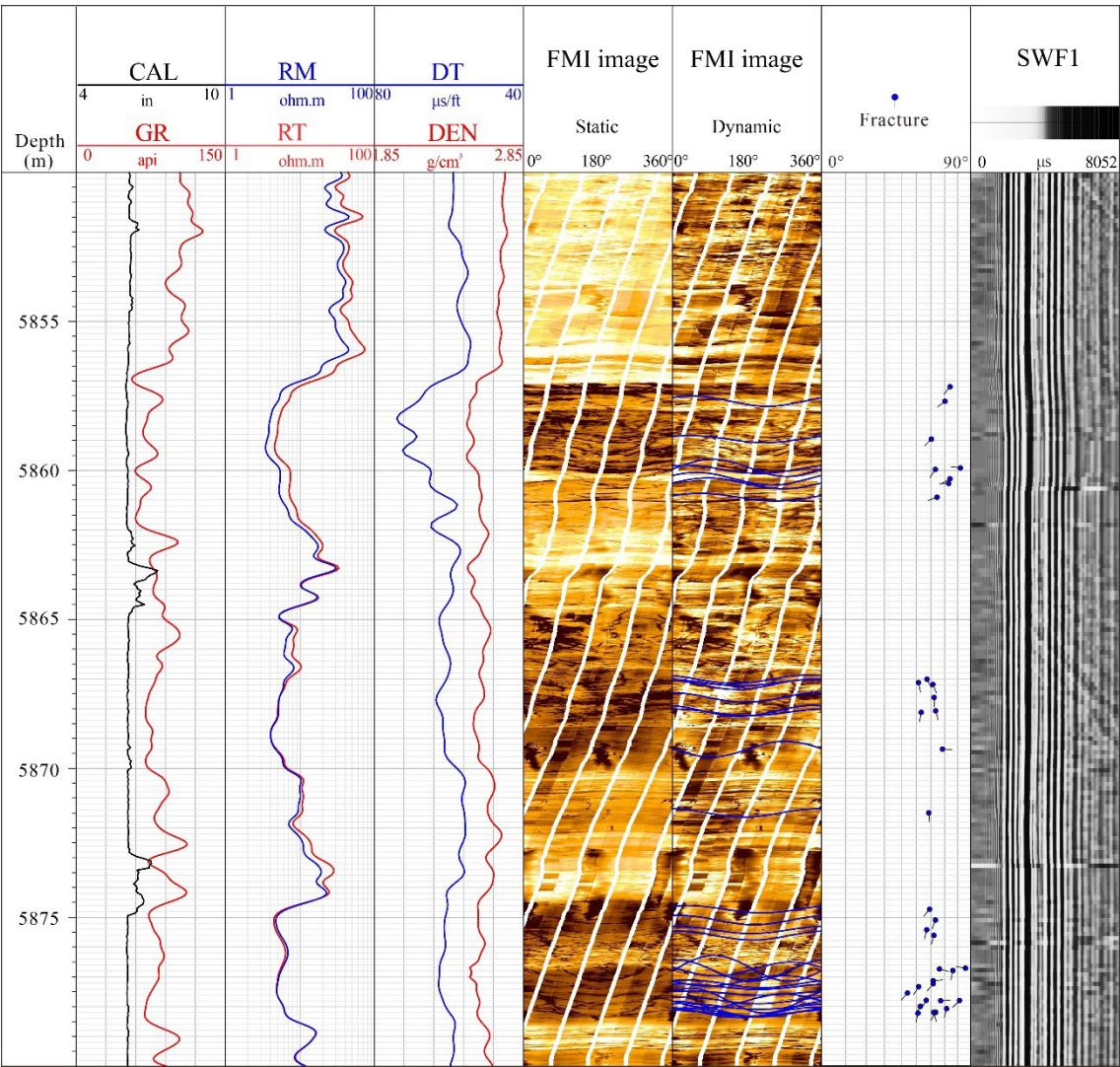


**Figure 4: The well log response of fracture in well logs including conventional well logs, image logs, and array acoustic logging in Well DB 1102**

#### 4.4 Sandbody controlled fracture distribution

##### 4.4.1 Sandstone-mudstone interfaces

Due to distinct mechanical properties of reservoirs in different lithologies, there are obvious differences in scale and occurrence of fractures generated by the same stress field (Laubach et al., 2009; Lucca et al., 2024). Fine-grained sandstones exhibited higher fracture densities compared with medium-grained sandstones and siltstones (Fig.5). Meanwhile, in medium-grained sandstones, there are also a multitude of fractures can be detected, but not as much as those in fine-grained sandstones.



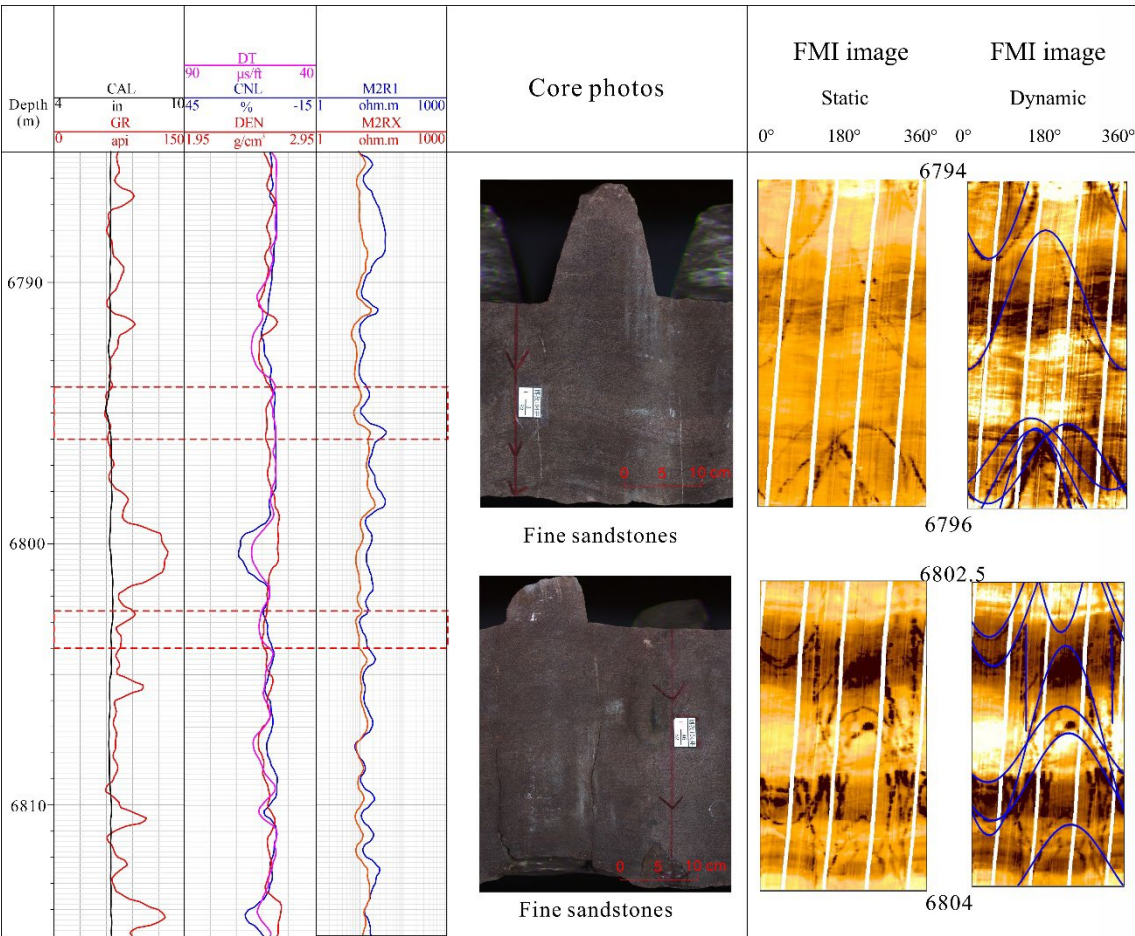


**Figure 5: The fracture characteristics in fine-grained sandstones (BZ 104)**

Due to the scarcity of core drilling data in Bozi-Dabei zone in Kuqa Depression, image logs are the primary technique for detecting fracture distribution at the interface of sandstone and mudstone. Fractures exhibit a composite pattern characterized by a longer extension when thick sandstone layers coexist with thin mudstone layers (Fig.6a, 6b). Conversely, when thin sandstone layers coexist with thicker mudstone layers, fractures manifest a shorter extension and less favorable connectivity (Fig.6c). The thickness of mudstones is related to the shorter extension of fractures (Fig.6). In conclusion, discrepancies in rock mechanics and relatively thin rock mechanic layers can restrict the formation of fractures.

Sandstones deform less under the same compression than mudstones, leading to localized tensile stress at their boundary due to transverse strain restriction (Biot et al., 1983; He et al., 2024). The presence of mudstone diminished the density of elastic strain energy in the sandstone at the lithological boundary, thereby limiting the formation of fractures (Feng et al., 2019).

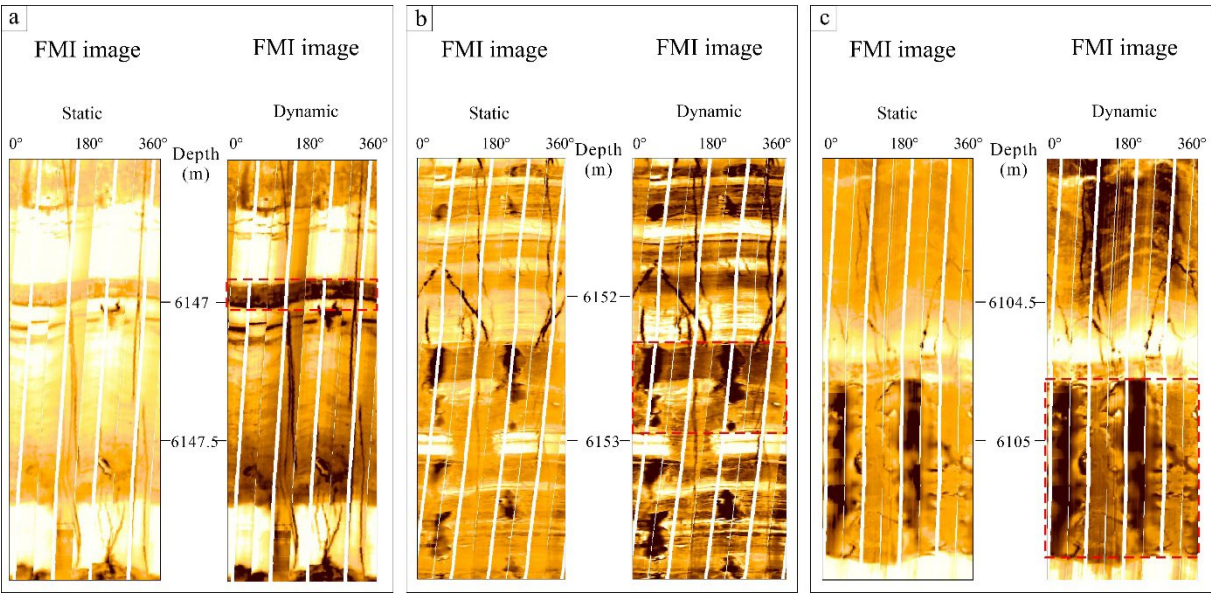


**Figure 6: The image logs revealing the characteristics within sand-mud interbeds**

225

**4.4.2 Sandbody thickness and fracture**

If the sandstones and mudstones suffer the approximate stress field, the elastic strain energy change would be closely related to the thickness (Feng et al., 2019; Smart et al., 2023). The average density of fractures tends to decrease with increasing sandbody thickness, i.e., the two parameters are negatively correlated (Fig.7). The thinner the layer, the more concentrated the stress at the fracture tip, and thinner sandbodies are more conducive to forming fractures (Griffith et al, 1921; Nian et al., 2017).

230

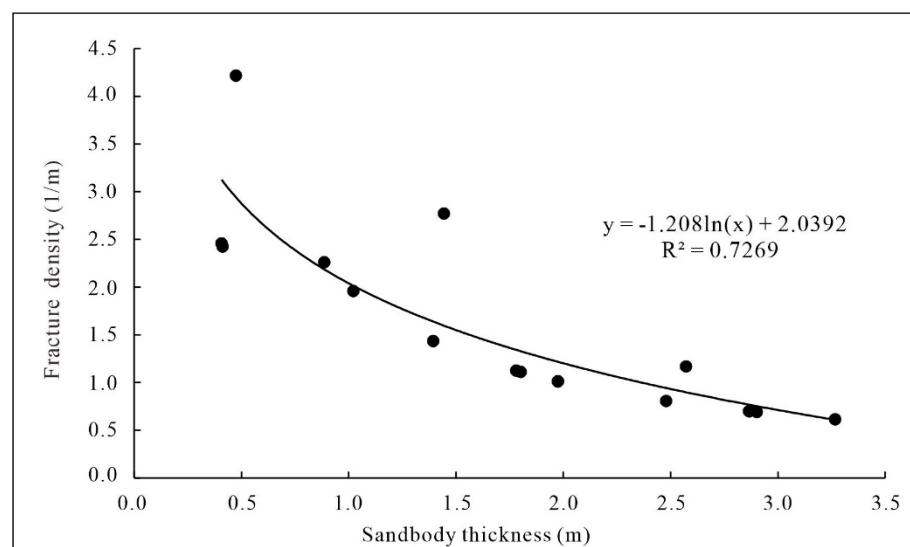


**Figure 7: The cross-plot of sandstone thickness versus fracture density**

#### 4.4.3 Fractures in various sandbodies

- 235 The interbedding of mudstone and sandstone layers plays a critical role in dictating fracture initiation potential. As illustrated in Figure 8, the mudstone's thickness in contact with the upper formation is a limiting factor for fracture propagation, with only 0.7 m thickness. In contrast, the mudstone thickness interbedded with the lower formation can extend up to 1.5 m, surpassing that of the upper formation. This increased thickness corresponds to a reduced elastic strain energy density, facilitating a higher incidence of forming fractures within the lower formation (Fig.8).
- 240 In summary, the lithological composition and sandbody thickness are identified as the primary controlling factors on fracture distribution. The lower sandbody thickness and lower mudstone thickness interfacing with the sandbody, as shown in Figure 8, indicate a higher potential for formation of fractures.



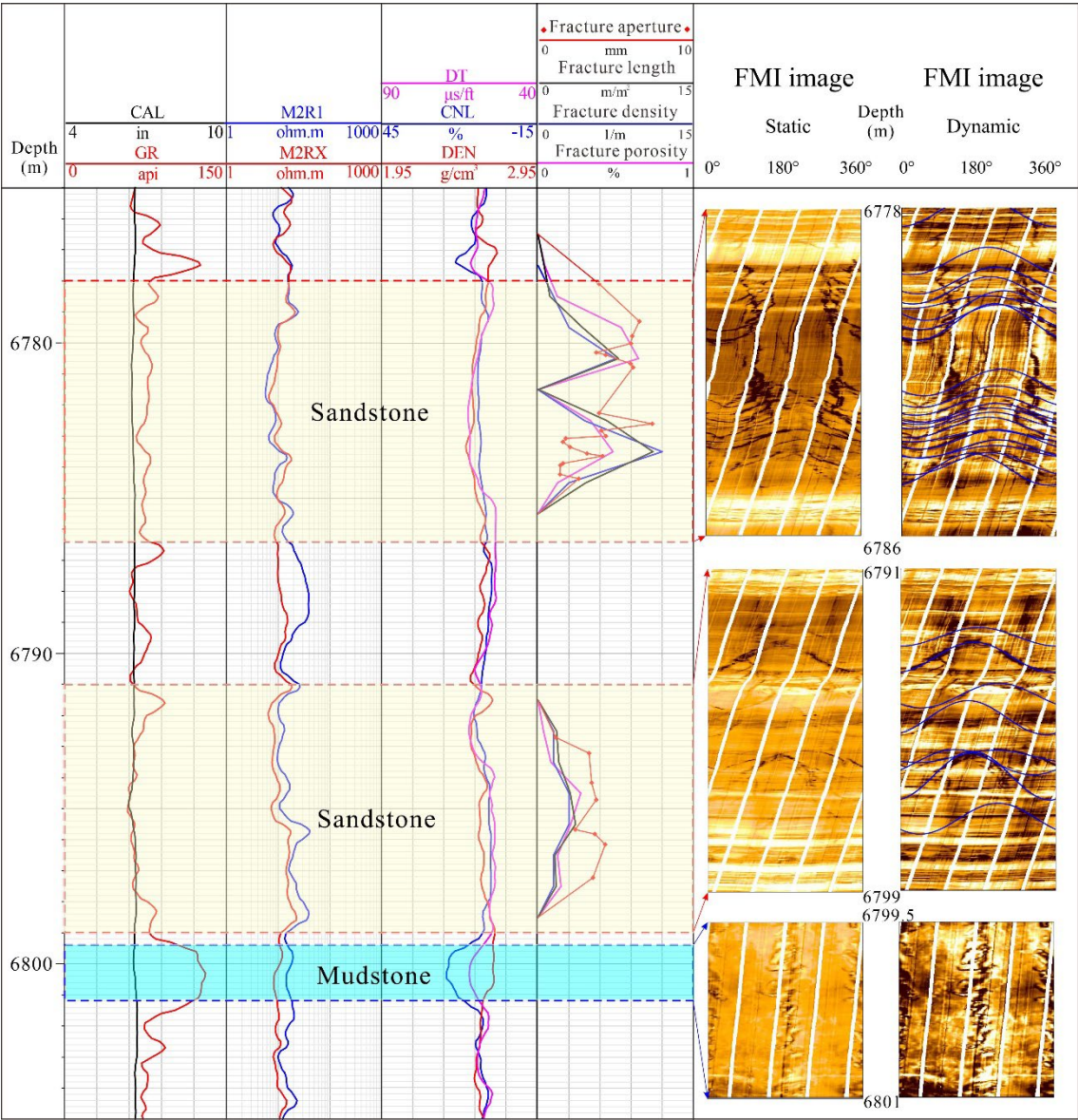


Figure 8: Characteristic comparison of fractures in different sandbodies in BZ 104

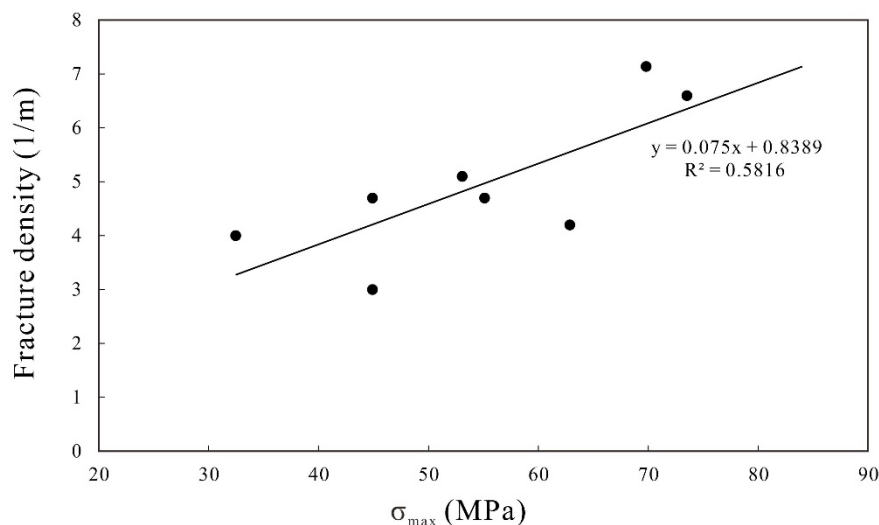
245 4.5 Paleostress and fracture density

Paleostress controls the generation and distribution of natural fractures. The paleostress magnitude is closely related to the formation of fractures (Liu et al., 2018; Zeng et al., 2023; Eichhubl and Aydin, 2023). The direction and intensity of paleostress field directly influence orientation and propagation of fractures within the rock formations (Zhang et al., 2022). By monitoring the material's response to stress, magnitude of maximum paleostress magnitude ( $\sigma_{max}$ ) can be obtained using AE tests. Core samples from Bashijiqike formation which are used for AE tests have similar rock composition, and the data indicate a positive

250



correlation between  $\sigma_{\max}$  and the fracture density (Fig.9). The high values of fracture density are mainly associated with high magnitude of  $\sigma_{\max}$ . In essence, an intensive paleostress is favorable for development of large-scale fractures in sandstones (Zeng et al., 2023).



255 **Figure 9: The cross-plot of fracture density versus maximum ancient stress**

#### 4.6 In situ stress magnitude and fracture distribution

In situ stress affects the late modification of natural fractures (Rajabi et al., 2010; Lai et al., 2019). The one-dimensional earth stress model is utilized to calculate the in-situ stress (Lai et al., 2022). The maximum principal horizontal stress (SHmax) magnitude, the minimum principal horizontal stress (SHmin) magnitude, and vertical principal stress (Sv) magnitude can be  
 260 calculated. Fracture aperture and intensity are controlled by the differences between maximum stress and minimum stress (SHmax-SHmin), actually fractures are easily to be kept open encountered with low horizontal stress differences. The results reveal that the in-situ stress field significantly controls the distribution of fractures. An obvious correlation has been found between fracture parameters (fracture aperture and porosity) and the magnitude of in situ stress (Fig.10). Higher fracture  
 265 parameters (fracture aperture and porosity) correspond to the lower  $\Delta\sigma/\text{SHmin}$  ( $\Delta\sigma/\text{SHmin}=(\text{SHmax}-\text{SHmin})/\text{SHmin}$ ) (Fig.10A, Fig.10B). As  $\Delta\sigma/\text{SHmin}$  gets higher, the difference in horizontal principal stresses is more obvious, and the magnitude of fracture parameter gets lower (Fig.10C). Therefore, in situ stress has a significant influence on the fracture aperture and porosity.

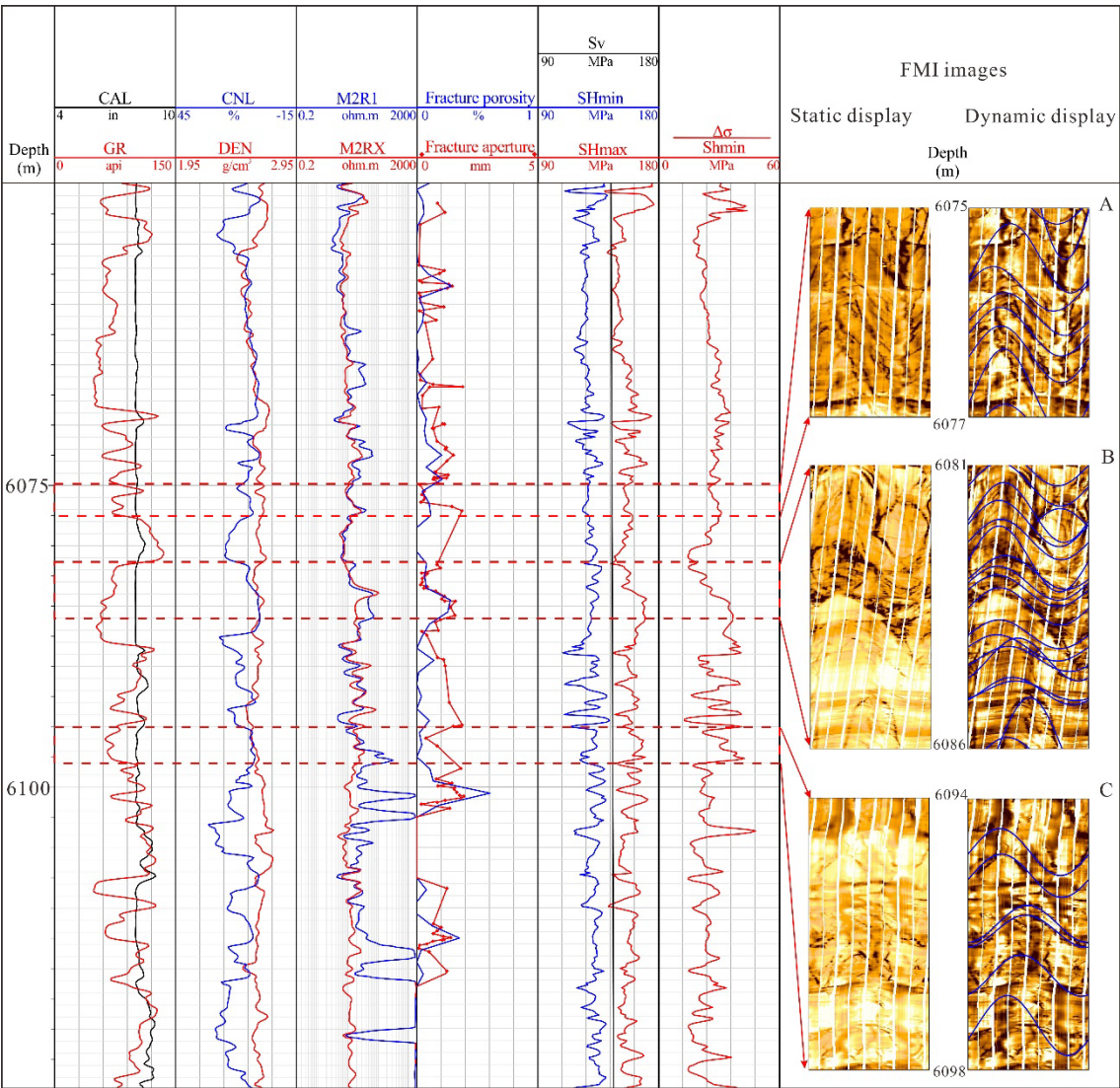


Figure 10: In situ stress magnitude and fracture parameters including fracture porosity and fracture aperture in Well BZ 17

270 **5 Discussion**

**5.1 Fracture distribution within structure positions**

The variations of fracture patterns are related to different structural position in a anticline and fault related anticline. The distribution of fractures is controlled by various structure position (Frehner et al., 2011; Cawood et al., 2023). The fractures are picked out in three wells of the BZ3 wellblock and the fracture parameters were calculated using image logs. The BZ 3 wellblock is located at a large-scale faulted anticline structure (Fig.11). Among them, the well BZ 3 and well BZ 301 are located near hinge of the anticline. In contrast, Well BZ 302 is located in the limb of the anticline (Fig.11). Due to the use of



oil-based mud drilling for BZ3 well, acoustic image log is utilized. The Well BZ 301 also uses oil-based mud for drilling, utilizing the Quatageo logs. However, the Well BZ 302 uses water-based muds for drilling, and the FMI logging tool is used. Affected by oil-based mud, the fractures in well BZ301 are more difficult to identify. Therefore, the fractures identified in BZ 3 and BZ 301 are fewer than the actual ones owing to the influence of oil-based muds using image logs (Fig.11).

The obvious phenomenon can be observed that the fractures detected in the upper strata are significantly more than those detected in the lower strata in each well (Fig.11). The fractures in upper neutral lines of the anticline are more numerous than those in below neutral lines of the anticline (Fig.11). The fractures in below neutral lines of anticline are much less developed, with lower fracture density and lower fracture apertures. Compressive stress tends to reduce the volume of the rock rather than increase the fracture aperture. However, fractures may be more developed due to tensile stress, with potentially higher fracture density and larger apertures in the upper part of an anticline (Jamison et al., 1997; Kim et al., 2022).

The production data and the fracture evaluation demonstrate that the amounts of fractures control the gas production rates and hydrocarbon accumulation conditions of reservoirs. The fracture density is a vital parameter to understand how the structure position controls fracture distribution. The higher fracture density corresponds to higher oil production. In the 5920-5958 m intervals in Well BZ 301, the oil test shows that the daily gas production is 494361 m<sup>3</sup> after blowout through a 7 mm choke whose fracture density is higher (5 /m). However, the daily gas production is 335302 m<sup>3</sup> after blowout through a 6 mm choke in Well BZ 3 whose fracture density is lower (2 /m) in the 5971.5-5985.5 m depth intervals (Fig.11).



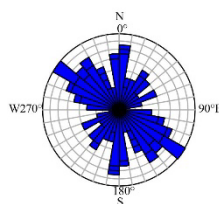
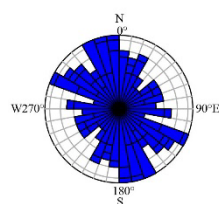
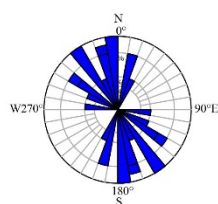
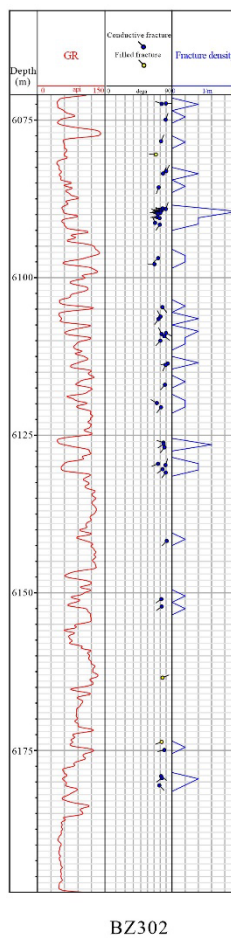
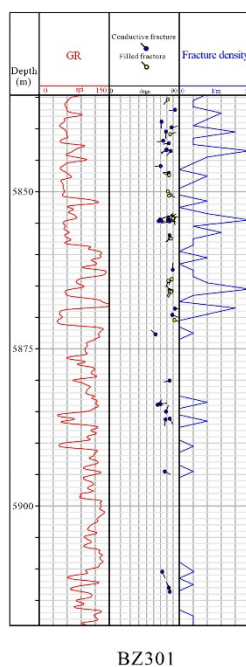
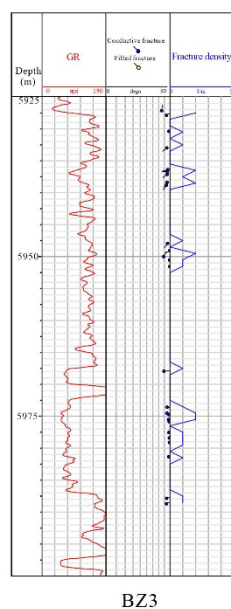
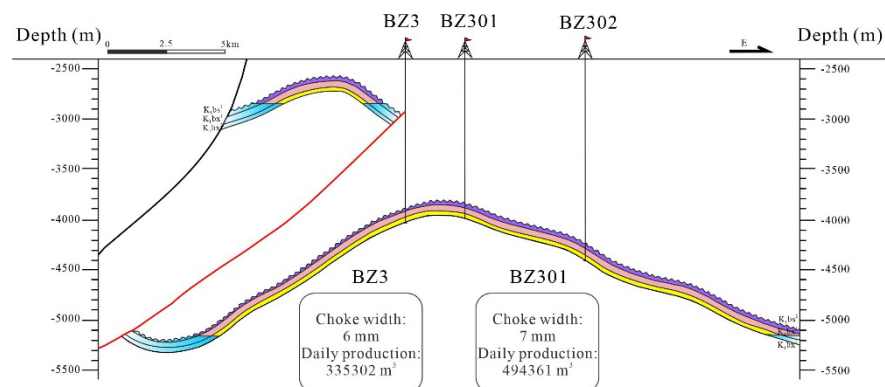






**Figure 11: Cross section of BZ 3 as well as fractures interpreted from image logs for BZ 3 wellblock**

295

300

305

310

Meanwhile, the 3 wells located in BZ 12 wellblock are both drilled in oil-based drilling muds. These wells use the same type of drilling muds, and can help evaluate fracture distribution in the anticline structure of the BZ 12 wellblock. The Well BZ 12 zone is located at a faulted-anticline structure. The distribution of fractures is not solely affected by the structural position but is also significantly affected by the proximity to fault, suggesting a complex multifactorial control within the geological setting (Fig.12) (Li et al., 2018). In the hinge of an anticline, due to the compression associated with folding, the concentration of stress is higher, which may lead to rock fracturing and fracture forming. In contrast, in the limbs of an anticline, the stress is more dispersed, hence fewer fractures form (McQuillan, 1973; Ghosh and Mitra, 2009; Cawood et al., 2023).

The amounts of fractures that are detected is the most in the Well BZ 1203, located at the hinge of the anticline, where the calculated fracture density (8/m) is high (Fig.12). In contrast, fewer fractures have been detected within the anticline's limbs, especially at Well BZ 1202. This is consistent with the conclusion that fracture density is strongly controlled by the position at anticlines. However, despite being located in the limb of the anticline, the fracture density at Well BZ 1201 is comparable to that of BZ 1203 in the hinge, as illustrated in Figure 12. The proximity of Well BZ 1201 to the fault is considered a contributing factor to the observed phenomenon. Meanwhile, seismic interpretation reveals that there is a fault near Well BZ 1201 (Fig. 13). This is the reason why, despite being located in the limb of the anticline, the Well BZ 1201 well exhibits a higher fracture density compared to the hinge of the anticline. Fractures are less prevalent in areas that are farther from the fault (Mitchell and Faulkner, 2012; Sun et al., 2021). The data reveal a positive correlation between gas production and fracture density within this geological setting. The high oil production corresponds to higher fracture densities (Fig. 12).

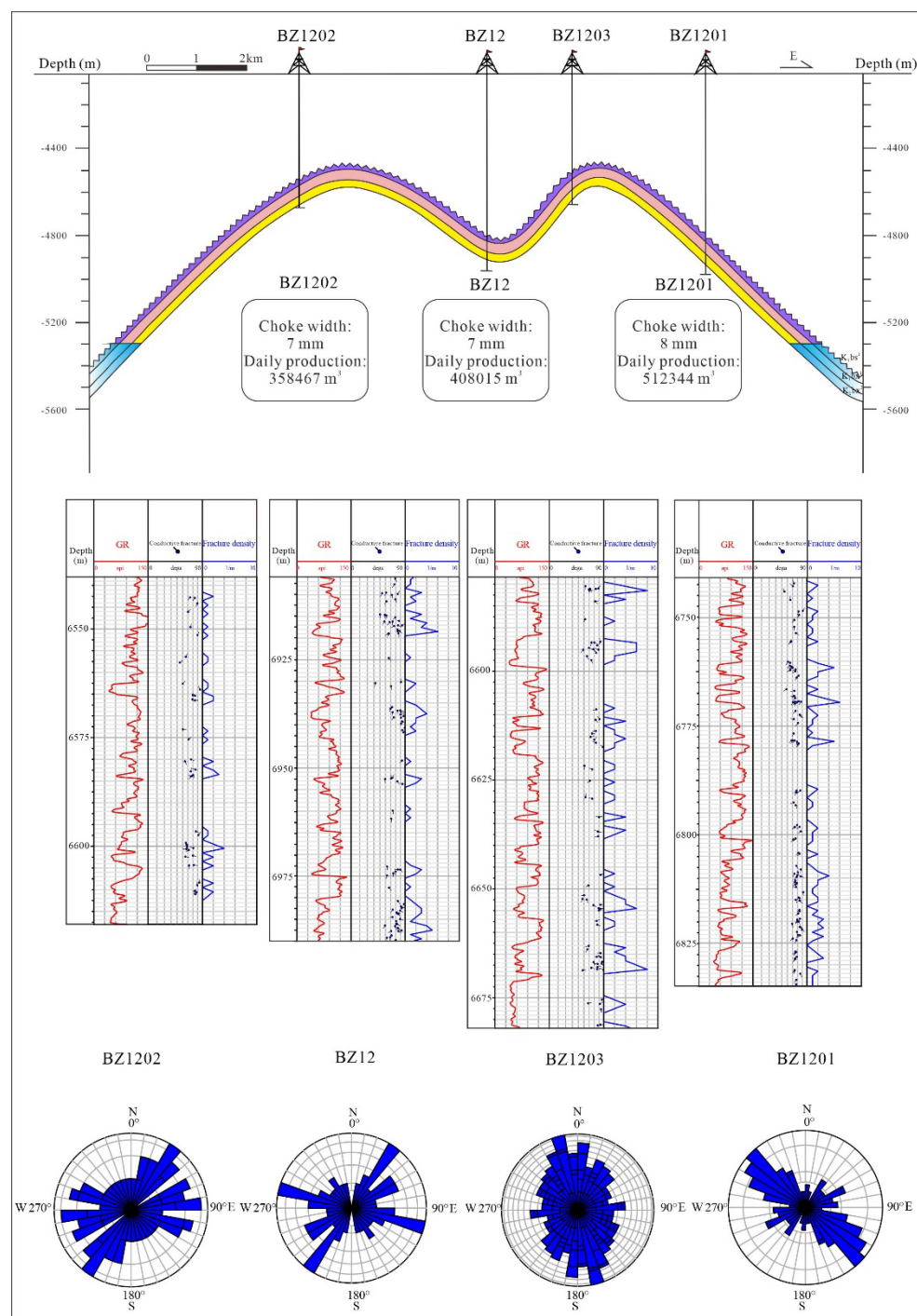


**Figure 12: Cross section of BZ 12 as well as fractures interpreted from image logs for BZ 12 wellblock**

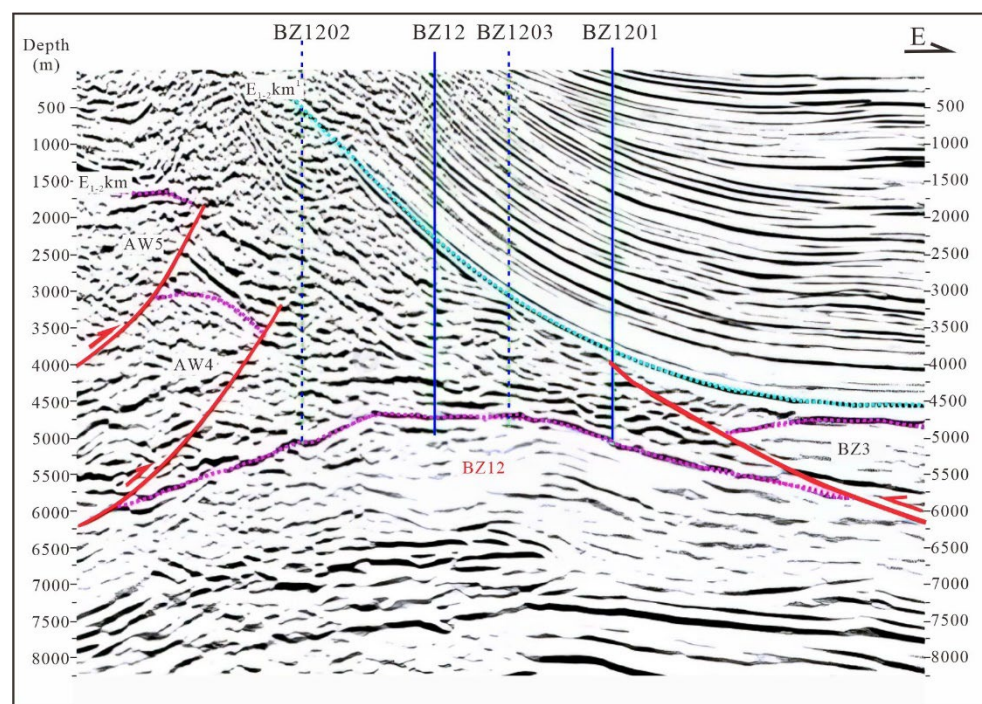


**Figure 13: Seismic profile and interpretation showing the main interpreted location of horizons and the faults in the BZ 12 wellblock**

## 5.2 Implication for hydrocarbon exploration

The strain distribution of the anticline can be delineated into three distinct zones including the extensional zone, the transitional zone, and the shortening zone by the presence of two neutral lines (Fig.14) (Frehner, 2011; Li et al., 2018). Then an analysis of the fracture distribution was conducted in the DB 9 wellblock in Kuqa Depression. The fracture distribution correlates with the structural position and will determine the well's production capacity.

The fractures detected in the upper strata above neutral lines, are significantly more than those detected in the lower strata in each well in the DB 9 wellblock. This phenomenon is particularly pronounced in extensional regions, where fracture density is significantly higher than in compressional areas. Notably, the magnitude of fractures is the highest in the well DB 9, which is situated at the hinge of an anticline.

Microscopic examination of thin sections indicates an absence of large pores due to the influence of a strong compressional stress field in well DB 9 (Anders et al., 2014; Li et al., 2018) (Fig.14). However, the presence of tensile fractures in both core samples and thin sections suggests that a regional tensile stress field has likely played a role in forming these open fractures in well DB 9 (Zeng, 2010; Haghi et al., 2019) (Fig.14). The presence of intragranular microfractures in well DB 902 is also related to tectonic compression (Anders et al., 2014) (Fig.14).

Furthermore, the statistics of fracture strikes and dips indicate that both the strikes and dips of fractures vary with structural position. The fracture dips are notably steep in DB 9 wellblock, particularly near the anticline's hinge. In contrast, fractures detected along the limb of the anticline exhibit relatively gentle dips. The strike of fractures in the hinge of the anticline is



oriented in parallel to the hinge line of the anticline owing to the concentration of the stress. However, their characteristics in  
335 the wings display relative variability.

The Well DB 9, as depicted in the fracture interpretation from image logs presented in Figure 14, has a higher fracture density.  
This well has demonstrated exceptional oil and gas productivity. In the 4802-4900 m depth intervals of Well DB 9, the oil test  
reveals that 511980 m<sup>3</sup> daily natural gas productivity is obtained with 8 mm choke width and drawdown pressure of 60.624  
MPa. The High-angle fractures are abundant and the fracture density is higher in this well interval. Grounded in empirical  
340 evidence, our study suggests the significant correlation between fracture density and oil production.



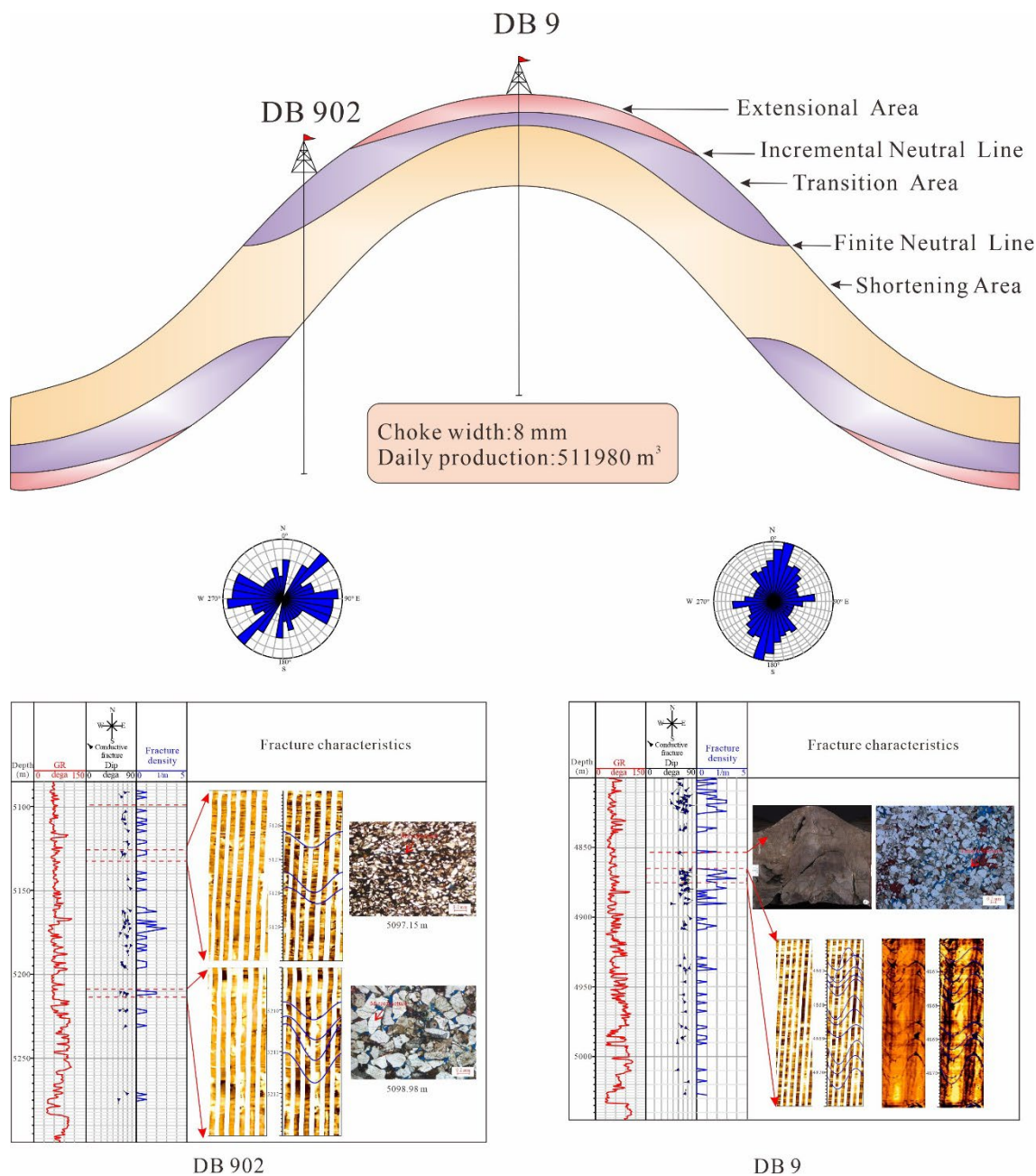


**Figure 14: The fracture characteristic in different structure position in anticline located at the DB 9 wellblock (Frehner, 2011; Li et al., 2018)**



## 345 6 Conclusions

This study unravels the geological factors controlling distribution of fractures integrating geological data and geophysical well logs. The fracture types can be categorized into five types including low-angle fractures, horizontal fractures, vertical fractures, high-angle fractures and fracture networks. High-angle fracture is the predominant type in Bozi-Dabei block. Fractures are particularly well-developed in fine-grained sandstones, which is the dominant rock type in the area. Sedimentary factors including sandbody thickness and sandstone-mudstone lithologic interface are the factors that affect the distribution of fractures. The fracture distribution is inversely related to the sandbody thickness, meaning that thicker sandbody tends to form fewer fractures. Conversely, the presence of thinner sandstones in conjunction with thin mud layers facilitates the formation of fractures. The earth stress is the factor that controls the fracture distribution. The findings indicate a positive correlation between the magnitude of the maximum paleostress and fracture density. An increase in the magnitude of the maximum paleostress corresponds to an increase in fracture density. In situ stress affects the late modification of natural fractures. An increase in the horizontal stress difference, reflecting a greater disparity between the horizontal principal stresses, leads to a decrease in fracture parameter magnitude. This implies that greater horizontal stress difference correlates with reduced fracture density.

The results and approaches of the study have some important implications for the structure position controlling the fracture distribution. Fractures in the hinge of an anticline are more abundant than those fractures in the limbs. The fracture density in the upper formations is higher along the longitudinal axis compared to the fracture density the lower formations. Besides the influence of anticline, fracture density is higher in the formation adjacent to the fault due to the effect of the regional stress field. Additionally, production data demonstrates that the presence of fractures enhances hydrocarbon productivity significantly. The higher fracture density corresponds to higher oil production.

365

### **Data availability**

The data used to support the findings of this study are available from the corresponding author upon request.

### **Author contributions**

YS, JL and GW contributed to the Conceptualization, Methodology, Software. WL, XJ and CH contributed to data curation and writing the original draft. YJ, ZR and LW contributed to the visualization and investigation. YS, JL and GW contributed to software and validation.

### **Competing interests**

The contact author has declared that neither they nor their co-authors have any competing interests.



375

## Disclaimer

Publisher's note: Copernicus Publications remains neutral with regard to jurisdictional claims in published maps and institutional affiliations.

## 380 Acknowledgments

This work is financially supported by National Natural Science Foundation of China (No. 41872133) and Science Foundation of China University of Petroleum, Beijing (No. 2462023QNXZ010). The authors thank PetroChina Tarim Oilfield Company for their data input to this work. We thank Hangzhou Institute of Geology, Research Institute of Petroleum Exploration and PetroChina Tarim Oilfield Company for their work.

385

## Financial support

This work is financially supported by National Natural Science Foundation of China (No. 41872133) and Science Foundation of China University of Petroleum, Beijing (No. 2462023QNXZ010). The authors thank PetroChina Tarim Oilfield Company for their data input to this work. We thank Hangzhou Institute of Geology, Research Institute of Petroleum Exploration and PetroChina Tarim Oilfield Company for their work.

390

## References

- Anders, M. H., Laubach, S. E., Scholz, C. H. 2014. Microfractures: A review. *Journal of Structural Geology*, 69, 377-394.
- Biot, M. A., Medlin, W. L., Masse, L. 1983. Fracture penetration through an interface. *Society of Petroleum Engineers Journal*, 23(6), 857-869.
- 395 Bogdonov, A. A. 1947. The intensity of cleavage as related to the thickness of beds. *Soviet Geology*, 16, 102-104.
- Cawood, A. J., Watkins, H., Bond, C. E., Warren, M. J., Cooper, M. A. 2023. Natural fracture patterns at Swift Reservoir anticline, NW Montana: the influence of structural position and lithology from multiple observation scales. *Solid earth*, 14(9), 1005-1030.
- Chen, S. J., Liu, Y., Zhang, J. C., Li, P., Tang, X., Li, Z. M., Dong, Z., Xu, L. F., Zhao, X. X. 2021. Formation conditions and evolution of fractures in multiple tight rocks: Implications for unconventional reservoir exploitation. *Journal of Petroleum Science and Engineering*, 200, 108354.
- 400



- Douma, L. A. N. R., Regelink, J. A., Bertotti, G., Boersma, Q. D., Barnhoorn, A. 2019. The mechanical contrast between layers controls fracture containment in layered rocks. *Journal of Structural Geology*, 127, 103856.
- Eichhubl, P., Aydin, A. 2003. Ductile opening-mode fracture by pore growth and coalescence during combustion alteration of siliceous mudstone. *Journal of Structural Geology*, 25(1), 121-134.
- 405 Feng, J., Liu, S., Du, H., Liu, H. 2023. Quantitative prediction of ultra-deep tight sandstone fractures based on the theory of minimum energy dissipation. *Geoenergy Science and Engineering*, 226, 211749.
- Feng, J., Shi, S., Zhou, Z., Li, X., Luo, P. 2019. Characterizing the influence of interlayers on the development and distribution of fractures in deep tight sandstones using finite element method. *Journal of Structural Geology*, 123, 81-95.
- 410 Frehner, M. 2011. The neutral lines in buckle folds. *Journal of Structural Geology*, 33(10), 1501-1508.
- Friedman, M. 1969. Structural Analysis of Fractures in Cores from Saticoy Field, Ventura County, California. *AAPG Bulletin*, 53(2), 367-389.
- Gale, J. F., Laubach, S. E., Olson, J. E., Eichhubl, P., Fall, A. 2014. Natural fractures in shale: A review and new observations. *AAPG Bulletin*, 98(11), 2165-2216.
- 415 Ghosh, K., Mitra, S. 2009. Structural controls of fracture orientations, intensity, and connectivity, Teton anticline, Sawtooth Range, Montana. *AAPG Bulletin*, 93(8), 995-1014.
- Griffith, A. A. 1921. VI. The phenomena of rupture and flow in solids. *Philosophical transactions of the royal society of london. Series A, containing papers of a mathematical or physical character*, 221(582-593), 163-198.
- Guo, P., Ren, D., Xue, Y. 2019. Simulation of multi-period tectonic stress fields and distribution prediction of tectonic fractures in tight gas reservoirs: A case study of the Tianhuan Depression in western Ordos Basin, China. *Marine and Petroleum Geology*, 109, 530-546.
- 420 Guo, X., Liu, K., Jia, C., Song, Y., Zhao, M., Zhuo, Q., Lu, X. 2016. Constraining tectonic compression processes by reservoir pressure evolution: Overpressure generation and evolution in the Kelasu Thrust Belt of Kuqa Foreland Basin, NW China. *Marine and Petroleum Geology*, 72, 30-44.
- 425 Haghi, A. H., Chalaturnyk, R., Talman, S. 2019. Stress-dependent pore deformation effects on multiphase flow properties of porous media. *Scientific Reports*, 9(1), 15004.
- Hanks, C. L., Lorenz, J., Teufel, L., Krumhardt, A. P. 1997. Lithologic and structural controls on natural fracture distribution and behavior within the Lisburne Group, northeastern Brooks Range and North Slope subsurface, Alaska. *AAPG Bulletin*, 81(10), 1700-1720.
- 430 He, Z., Wu, G., Zhu, J. 2024. Mechanical properties of rock under uniaxial compression tests of different control modes and loading rates. *Scientific Reports*, 14(1), 2164.
- Ishii, E., Sanada, H., Funaki, H., Sugita, Y., Kurikami, H. 2011. The relationships among brittleness, deformation behavior, and transport properties in mudstones: An example from the Horonobe Underground Research Laboratory, Japan. *Journal of Geophysical Research: Solid Earth*, 116(B9).





- 435 Jamison, W. R. 1997. Quantitative Evaluation of Fractures on Monkshood Anticline, a Detachment Fold in the Foothills of Western Canada. AAPG Bulletin, 81(7), 1110-1132.
- Jia, C. Z., Li, Q. M. 2008. Petroleum geology of Kela-2, the most productive gas field in China. Marine and Petroleum Geology, 25(4-5), 335-343.
- Ju, W., Hou, G., Zhang, B. 2014. Insights into the damage zones in fault-bend folds from geomechanical models and field data. Tectonophysics, 610, 182-194.
- 440 Kaiser J., 1953. Erkenntnisse und Folgerungen aus der Messung von Geräuschen bei Zugbeanspruchung von metallischen Werkstoffen, Arch. Eisenhütten., 24, 1-2.
- Kim, I., Park, S. I., Kwon, S., Lee, H. J. 2022. Evolution of fracture networks and connectivity during fault-bend folding: Insights from the Sinon Anticline in the southwestern Hongseong-Imjingang Belt, Korea. Journal of Structural Geology, 155, 104506.
- 445 Koerperich, E. A. 1978. Investigation of Acoustic Boundary Waves And Interference Patterns as Techniques for Detecting Fractures. Journal of Petroleum Technology, 30(8), 1199-1207.
- Lai J., Su Y., Xiao L., Zhao F., Bai T., Li Y., Li H., Huang Y., Wang G., Qin Z. 2024. Application of geophysical well logs in solving geologic issues: Past, present and future prospect. Geoscience Frontiers, 15, 101779.
- 450 Lai J., Wang G., Fan Q., Zhao F., Zhao X., Li Y., Zhao Y., Pang X. 2023. Towards the scientific interpretation of geophysical well logs: typical misunderstandings and countermeasures. Surveys in Geophysics, 44: 463-494
- Lai, J., Chen, K., Xin, Y., Wu, X., Chen, X., Yang, K., Song, Q., Wang, G., Ding, X. 2021. Fracture characterization and detection in the deep Cambrian dolostones in the Tarim Basin, China: Insights from borehole image and sonic logs. Journal of Petroleum Science and Engineering, 196, 107659.
- 455 Lai, J., Li, D., Wang, G., Xiao, C., Hao, X., Luo, Q., Lai, L., Qin, Z. 2019. Earth stress and reservoir quality evaluation in high and steep structure: The Lower Cretaceous in the Kuqa Depression, Tarim Basin, China. Marine and Petroleum Geology, 101, 43-54.
- Lai, J., Wang, G., Wang, S., Cao, J., Li, M., Pang, X., Han, C., Fan, X., Yang, L., He, Z., Qin, Z. 2018. A review on the applications of image logs in structural analysis and sedimentary characterization. Marine and Petroleum Geology, 95, 139-166.
- 460 Lai J., Wang G., Chai Y., Xin Y., Wu Q., Zhang X., Sun Y. 2017. Deep burial diagenesis and reservoir quality evolution of high-temperature, high-pressure sandstones: Examples from Lower Cretaceous Bashijiqike Formation in Keshen area, Kuqa depression, Tarim basin of China. AAPG Bulletin, 101(6): 829-862.
- Laubach, S. E. 2003. Practical approaches to identifying sealed and open fractures. AAPG Bulletin, 87(4), 561-579.
- 465 Laubach, S. E., Lander, R. H., Criscenti, L. J., Anovitz, L. M., Urai, J. L., Pollyea, R. M., et al. 2019. The role of chemistry in fracture pattern development and opportunities to advance interpretations of geological materials. Reviews of Geophysics, 57, 1065-1111.
- Laubach, S. E., Olson, J. E., Gross, M. R. 2009. Mechanical and fracture stratigraphy. AAPG Bulletin, 93(11), 1413-1426.



- Lavrov, A. 2003. The Kaiser effect in rocks: Principles and stress estimation techniques. *International Journal of Rock Mechanics and Mining Sciences*, 40(2), 151-171.
- Li, P., Lee J., Taher A., Coates R., Marlow R. 2019. "New 4 3/4-In. High-Resolution Ultrasonic Borehole Imaging for Unconventional Reservoir Evaluation." In *Unconventional Resources Technology Conference*, Denver, Colorado, 22-24 July 2019, SEG Global Meeting Abstracts, Unconventional Resources Technology Conference (URTeC); Society of Exploration Geophysicists, 43–61.
- Li, Y. J., Wen, L., Zhang, H. A., Huang, T. Z., Li, H. L., Shi, Y. Y., Meng, Q. L., Peng, G. X., Huang, S. Y., Zhang, Q. 2016. The Kuqa late Cenozoic fold–thrust belt on the southern flank of the Tian Shan Mountains. *International Journal of Earth Sciences*, 105(5), 1417-1430.
- Li, Y., He, J., Deng, H., Li, R., Li, Q., Fu, M., Yu, Y. 2024. Effect of lithofacies assemblages on multi-scale fractures in the transitional shale and its implications for shale gas exploration. *Geoenergy Science and Engineering*, 233, 212562.
- Li, Y., Hou, G., Hari, K. R., Neng, Y., Lei, G., Tang, Y., Zhou, L., Sun, S., Zheng, C. 2018. The model of fracture development in the faulted folds: The role of folding and faulting. *Marine and Petroleum Geology*, 89, 243-251.
- Liu, J., Ding, W., Gu, Y., Xiao, Z., Dai, J., Dai, P., Chen, X., Zhao, G. 2018. Methodology for predicting reservoir breakdown pressure and fracture opening pressure in low-permeability reservoirs based on an in situ stress simulation. *Engineering Geology*, 246, 222-232.
- Liu, L., Pan, H. P., Lin, Z. Z., Zhang, S. H., Qin, Z., Li, J. W., Huang, G. S., Wang, L., Li, D. 2020. Reservoir characteristics and logging evaluation of gas-bearing mudstone in the south of north china plain. *Scientific reports*, 10(1), 8791.
- Lucca, A., Ogata, K., Balsamo, F., Borsani, A., Clemenzi, L., Hatushika, R., Tinterri, R., Storti, F. 2024. Sedimentary facies control on fracture and mechanical stratigraphy in siliciclastics: Marnoso-arenacea formation, Northern Apennines, Italy. *Marine and Petroleum Geology*, 167, 106927.
- Lyu, W., Zeng, L., Liu, Z., Liu, G., Zu, K. 2016. Fracture responses of conventional logs in tight-oil sandstones: A case study of the Upper Triassic Yanchang Formation in southwest Ordos Basin, China. *AAPG Bulletin*, 100(9), 1399-1417.
- Lyu, W., Zeng, L., Lyu, P., Yi, T., Dong, S., Wang, S., Xu, X., Chen, H. 2022. Insights into the mechanical stratigraphy and vertical fracture patterns in tight oil sandstones: The Upper Triassic Yanchang Formation in the eastern Ordos Basin, China. *Journal of Petroleum Science and Engineering*, 212, 110247.
- Maleki, S., Moradzadeh, A., Ghavami Riabi, R., Sadaghzadeh, F. 2014. Comparison of Several Different Methods of in situ stress determination. *International Journal of Rock Mechanics and Mining Sciences*, 71, 395-404.
- McQuillan, H. 1973. Small-Scale Fracture Density in Asmari Formation of Southwest Iran and Its Relation to Bed Thickness and Structural Setting1. *AAPG Bulletin* 57(12): 2367-85.
- Mitchell, T. M., Faulkner, D. R. 2012. Towards quantifying the matrix permeability of fault damage zones in low porosity rocks. *Earth and Planetary Science Letters*, 339-340, 24-31.
- Najibi, A. R., Ghafoori, M., Lashkaripour, G. R., Asef, M. R. 2017. Reservoir geomechanical modeling: In-situ stress, pore pressure, and mud design. *Journal of Petroleum Science and Engineering*, 151, 31-39.



- Nelson, R. A. 1985. Geologic analysis of naturally fractured reservoirs (Vol. 1). Gulf Professional Publishing.
- Nian, T., Wang, G., Song, H. 2017. Open tensile fractures at depth in anticlines: A case study in the Tarim basin, NW China. *Terra Nova*, 29(3), 183-190.
- Ogata, K., Storti, F., Balsamo, F., Tinterri, R., Bedogni, E., Fetter, M., Gomes, L., Hatushika, R. 2017. Sedimentary facies control on mechanical and fracture stratigraphy in turbidites. *GSA Bulletin*, 129(1-2), 76-92.
- Olson, J. E., Laubach, S. E., Lander, R. H. 2009. Natural fracture characterization in tight gas sandstones: Integrating mechanics and diagenesis. *AAPG Bulletin*, 93(11), 1535-1549.
- Pang, X., Wang, G., Kuang, L., Lai, J., Mountney, N. P. 2024. Investigation of Fluid Types in Shale Oil Reservoirs. *Surveys in Geophysics*.
- Peng, K., Feng, K., Chen, B., Shan, Y., Zhang, N., Wang, P., Fang, K., Bai, Y., Zou, X., Wei, W., Geng, X., Zhang, Y., Li, J. 2023. The global power sector's low-carbon transition may enhance sustainable development goal achievement. *Nature Communications*, 14(1), 3144.
- Qiu, N., Chang, J., Zuo, Y., Wang, J., Li, H. 2012. Thermal evolution and maturation of lower Paleozoic source rocks in the Tarim Basin, northwest China. *AAPG Bulletin*, 96(5), 789-821.
- Rajabi M., Sherkati S., Bohloli B., Tingay M., 2010. Subsurface fracture analysis and determination of in-situ stress direction using FMI logs: An example from the Santonian carbonates (Ilam Formation) in the Abadan Plain, Iran. *Tectonophysics* 492, 192-200.
- Smart, K. J., Ferrill, D. A., Morris, A. P. 2023. Geomechanical insights on the importance of mechanical stratigraphy to hydraulic fracture containment. *AAPG Bulletin*, 107(10), 1811-1835.
- Sun, X., Gomez-Rivas, E., Alcalde, J., Martín-Martín, J. D., Ma, C., Muñoz-López, D., Cruset, D., Cantarero, I., Grier, A., Travé, A. 2021. Fracture distribution in a folded fluvial succession: The Puig-reig anticline (south-eastern Pyrenees). *Marine and Petroleum Geology*, 132, 105169.
- Watkins, H., Butler, R. W. H., Bond, C. E., Healy, D. 2015. Influence of structural position on fracture networks in the Torridon Group, Achnashellach fold and thrust belt, NW Scotland. *Journal of Structural Geology*, 74, 64-80.
- Yang, K., Xu, L., Qi, J., He, P., Du, J., Sun, T. 2023. Structural deformation of the Northern Monocline belt in the Kuqa depression and implications for the Cenozoic uplift history of the South Tianshan Mountains. *Tectonophysics*, 857, 229840.
- Yang, Y., Li, X., Yang, X., Li, X. 2022. Influence of reservoirs/interlayers thickness on hydraulic fracture propagation laws in low-permeability layered rocks. *Journal of Petroleum Science and Engineering*, 219, 111081.
- Yu, S., Chen, W., Evans, N. J., McInnes, B. I. A., Yin, J., Sun, J., Li, J., 2014. Cenozoic uplift, exhumation, and deformation in the north Kuqa Depression, China as constrained by (U-Th)/He thermochronometry. *Tectonophysics*, 630, 166-182.
- Zahmatkesh, I., Soleimani, B., Kadkhodaie, A., Golalzadeh, A., Abdollahi, A.-M. 2017. Estimation of DSI log parameters from conventional well log data using a hybrid particle swarm optimization–adaptive neuro-fuzzy inference system. *Journal of Petroleum Science and Engineering*, 157, 842-859.



- Zeng, L. 2010. Microfracturing in the Upper Triassic Sichuan Basin tight-gas sandstones: Tectonic, overpressure, and diagenetic origins. *AAPG Bulletin*, 94(12), 1811-1825.
- Zeng, L., Gong, L., Zhang, Y., Dong, S., Lyu, W. 2023. A review of the genesis, evolution, and prediction of natural fractures in deep tight sandstones of China. *AAPG Bulletin*, 107(10), 1687-1721.
- 540 Zeng, L., Su, H., Tang, X., Peng, Y., Gong, L. 2013. Fractured tight sandstone oil and gas reservoirs: A new play type in the Dongpu depression, Bohai Bay Basin, China. *AAPG Bulletin*, 97(3), 363-377.
- Zhang, D., Tang, J., Chen, K., Wang, K., Zhang, P., He, G., Tuo, X. 2022. Simulation of tectonic stress field and prediction of tectonic fracture distribution in Longmaxi Formation in Lintanchang area of eastern Sichuan Basin. *Frontiers in Earth Science*, 10, 1024748.
- 545 Zhang, G., Liu, J., Xu, K., Jiang, S., Zhang, B., Shi, N. 2024. Characteristics and effectiveness of deep and ultradeep tight sandstone fractures: Insights from geological and geophysical data analysis. *Geophysics*, 89(5), 1-55.
- Zhang, Y., Zhang, J., Xia, Y., He, Y. 2023. Fracture identification and characteristics of carbonate underground gas storage: an example from the eastern area of Sulige gas field, ordos Basin, China. *Scientific Reports*, 13(1), 22446.
- Zhao, F., Shi, Z., Yu, S., Zheng, H. 2023. A review of fracture mechanic behaviors of rocks containing various defects. *Underground Space*, 12, 102-115.
- 550 Zhao, Z., He, Y., Huang, X. 2021. Study on Fracture Characteristics and Controlling Factors of Tight Sandstone Reservoir: A Case Study on the Huagang Formation in the Xihu Depression, East China Sea Shelf Basin, China. *Lithosphere*, 2021(Special 1), 3310886.
- Zoback, M. D., Barton, C. A., Brudy, M., Castillo, D. A., Finkbeiner, T., Grollmund, B. R., Moos, D. B., Peska, P., Ward, C. D., Wiprut, D. J. 2003. Determination of stress orientation and magnitude in deep wells. *International Journal of Rock Mechanics and Mining Sciences*, 40(7), 1049-1076.